Femtosecond laser induced structural changes in fluorozirconate glass

Simon Gross,[1,*] **David G. Lancaster,**[2] **Heike Ebendorff-Heidepriem,**[2] **Tanya M. Monro,**[2] **Alexander Fuerbach,**[1] **and Michael J. Withford**[1]

[1]*Centre for Ultrahigh-bandwidth Devices for Optical Systems (CUDOS) and MQ Photonics Research Centre, Department of Physics and Astronomy, Macquarie University, New South Wales, 2109, Australia*

[2]*IPAS and School of Chemistry & Physics, University of Adelaide, South Australia, 5005, Australia*

[*]*simon.gross@mq.edu.au*

Abstract: Fluorozirconate glasses, such as ZBLAN (ZrF_4-BaF_2-LaF_3-AlF_3-NaF), have a high infrared transparency and large rare-earth solubility, which makes them an attractive platform for highly efficient and compact mid-IR waveguide lasers. We investigate the structural changes within the glass network induced by high repetition rate femtosecond laser pulses and reveal the origin of the observed decrease in refractive index by using Raman microscopy. The high repetition rate pulse train causes local melting followed by rapid quenching of the glass network. This results in breaking of bridging bonds between neighboring zirconium fluoride polyhedra and as the glass resolidifies, a larger fraction of single bridging fluorine bonds relative to double bridging links are formed in comparison to the pristine glass. The distance between adjacent zirconium cations is larger for single bridging than double bridging links and consequently an expansion of the glass network occurs. The rarified glass network can be related to the experimentally observed decrease in refractive index via the Lorentz-Lorenz equation.

OCIS codes: (140.3390) Laser materials processing; (320.2250) Femtosecond phenomena; (260.5210) Photoionization; (160.2750) Glass and other amorphous materials; (300.6450) Spectroscopy, Raman.

References and links

1. R. R. Gattass and E. Mazur, "Femtosecond laser micromachining in transparent materials," Nat. Photonics **2**, 219–225 (2008).
2. S. M. Eaton, W. Chen, L. Zhang, H. Zhang, R. Iyer, J. Aitchison, and P. Herman, "Telecom-band directional coupler written with femtosecond fiber laser," IEEE Photon. Technol. Lett. **18**, 2174–2176 (2006).
3. G. D. Marshall, A. Politi, J. C. F. Matthews, P. Dekker, M. Ams, M. J. Withford, and J. L. O'Brien, "Laser written waveguide photonic quantum circuits," Opt. Express **17**, 12546–12554 (2009).
4. R. M. Vazquez, R. Osellame, D. Nolli, C. Dongre, H. van den Vlekkert, R. Ramponi, M. Pollnau, and G. Cerullo, "Integration of femtosecond laser written optical waveguides in a lab-on-chip," Lab Chip **9**, 91–96 (2009).
5. R. R. Thomson, A. K. Kar, and J. Allington-Smith, "Ultrafast laser inscription: an enabling technology for astrophotonics," Opt. Express **17**, 1963–1969 (2009).
6. M. Ams, G. D. Marshall, P. Dekker, J. A. Piper, and M. J. Withford, "Ultrafast laser written active devices," Laser Photon. Rev. **3**, 535–544 (2009).
7. D. J. Little, M. Ams, P. Dekker, G. D. Marshall, J. M. Dawes, and M. J. Withford, "Femtosecond laser modification of fused silica: the effect of writing polarization on Si-O ring structure," Opt. Express **16**, 20029–20037 (2008).

#185229 - $15.00 USD Received 11 Feb 2013; revised 25 Mar 2013; accepted 26 Mar 2013; published 5 Apr 2013

8. L. B. Fletcher, J. J. Witcher, N. Troy, S. T. Reis, R. K. Brow, and D. M. Krol, "Direct femtosecond laser waveguide writing inside zinc phosphate glass," Opt. Express **19**, 7929–7936 (2011).
9. J. Chan, T. Huser, S. Risbud, and D. M. Krol, "Modification of the fused silica glass network associated with waveguide fabrication using femtosecond laser pulses," Appl. Phys. A: Mater. Sci. Process. **76**, 367–372 (2003).
10. W. J. Reichman, D. M. Krol, L. Shah, F. Yoshino, A. Arai, S. M. Eaton, and P. R. Herman, "A spectroscopic comparison of femtosecond-laser-modified fused silica using kilohertz and megahertz laser systems," J. Appl. Phys. **99**, 123112 (2006).
11. D. M. Krol, "Femtosecond laser modification of glass," J. Non-Cryst. Solids **354**, 416–424 (2008).
12. J. W. Chan, T. Huser, S. Risbud, and D. M. Krol, "Structural changes in fused silica after exposure to focused femtosecond laser pulses," Opt. Lett. **26**, 1726–1728 (2001).
13. A. M. Streltsov and N. F. Borrelli, "Study of femtosecond-laser-written waveguides in glasses," J. Opt. Soc. Am. B **19**, 2496–2504 (2002).
14. F. Vega, J. Armengol, V. Diez-Blanco, J. Siegel, J. Solis, B. Barcones, A. Perez-Rodriguez, and P. Loza-Alvarez, "Mechanisms of refractive index modification during femtosecond laser writing of waveguides in alkaline lead-oxide silicate glass," Appl. Phys. Lett. **87**, 021109 (2005).
15. D. J. Little, M. Ams, S. Gross, P. Dekker, C. T. Miese, A. Fuerbach, and M. J. Withford, "Structural changes in BK7 glass upon exposure to femtosecond laser pulses," J. Raman Spectrosc. **42**, 715–718 (2011).
16. L. B. Fletcher, J. J. Witcher, W. B. Reichman, A. Arai, J. Bovatsek, and D. M. Krol, "Changes to the network structure of Er-Yb doped phosphate glass induced by femtosecond laser pulses," J. Appl. Phys. **106**, 083107 (2009).
17. D. J. Little, M. Ams, P. Dekker, G. D. Marshall, and M. J. Withford, "Mechanism of femtosecond-laser induced refractive index change in phosphate glass under a low repetition-rate regime," J. Appl. Phys. **108**, 033110 (2010).
18. A. Zoubir, M. Richardson, C. Rivero, A. Schulte, C. Lopez, K. Richardson, N. Hô, and R. Vallée, "Direct femtosecond laser writing of waveguides in As2S3 thin films," Opt. Lett. **29**, 748–750 (2004).
19. L. Petit, N. Carlie, T. Anderson, M. Richardson, and K. Richardson, "Progress on the photoresponse of chalcogenide glasses and films to near-infrared femtosecond laser irradiation: a review," IEEE J. Sel. Top. Quantum Electron. **14**, 1323–1334 (2008).
20. R. K. Brow, "Review: the structure of simple phosphate glasses," J. Non-Cryst. Solids **263-264**, 1–28 (2000).
21. F. Gan, "Optical properties of fluoride glasses: a review," J. Non-Cryst. Solids **184**, 9–20 (1995).
22. V. K. Bogdanov, W. E. K. Gibbs, D. J. Booth, J. S. Javorniczky, P. J. Newman, and D. R. MacFarlane, "Fluorescence from highly-doped erbium fluorozirconate glasses pumped at 800 nm," Opt. Commun. **132**, 73–76 (1996).
23. D. G. Lancaster, S. Gross, A. Fuerbach, H. E. Heidepriem, T. M. Monro, and M. J. Withford, "Versatile large-mode-area femtosecond laser-written Tm:ZBLAN glass chip lasers," Opt. Express **20**, 27503–27509 (2012).
24. S. H. Wiersma, P. Török, T. D. Visser, and P. Varga, "Comparison of different theories for focusing through a plane interface," J. Opt. Soc. Am. A **14**, 1482–1490 (1997).
25. H. Ebendorff-Heidepriem, T.-C. Foo, R. C. Moore, W. Zhang, Y. Li, T. M. Monro, A. Hemming, and D. G. Lancaster, "Fluoride glass microstructured optical fiber with large mode area and mid-infrared transmission," Opt. Lett. **33**, 2861–2863 (2008).
26. C. Schaffer, J. García, and E. Mazur, "Bulk heating of transparent materials using a high-repetition-rate femtosecond laser," Appl. Phys. A: Mater. Sci. Process. **76**, 351–354 (2003).
27. S. M. Eaton, H. Zhang, M. L. Ng, J. Li, W.-J. Chen, S. Ho, and P. R. Herman, "Transition from thermal diffusion to heat accumulation in high repetition rate femtosecond laser writing of buried optical waveguides," Opt. Express **16**, 9443–9458 (2008).
28. O. F. Nielsen, *Low-Frequency Raman Spectroscopy and Biomolecular Dynamics: A Comparison Between Different Low-Frequency Experimental Techniques. Collectivity of Vibrational Modes*, 1st ed. (CRC Press, 2001), Chap. 15.
29. R. M. Almeida and J. D. Mackenzie, "Vibrational spectra and structure of fluorozirconate glasses," J. Chem. Phys. **74**, 5954–5961 (1981).
30. Y. Kawamoto and F. Sakaguchi, "Thermal properties and Raman spectra of crystalline and vitreous BaZrF6, PbZrF6, and SrZrF6," Bull. Chem. Soc. Jpn. **56**, 2138–2141 (1983).
31. Y. Kawamoto, T. Horisaka, K. Hirao, and N. Soga, "A molecular dynamics study of barium meta-fluorozirconate glass," J. Chem. Phys. **83**, 2398–2404 (1985).
32. C. C. Phifer, C. Austen Angell, J. Laval, and J. Lucas, "A structural model for prototypical fluorozirconate glass," J. Non-Cryst. Solids **94**, 315–335 (1987).
33. B. Boulard, J. Kieffer, C. C. Phifer, and C. Angell, "Vibrational spectra in fluoride crystals and glasses at normal and high pressures by computer simulation," J. Non-Cryst. Solids **140**, 350–358 (1992).
34. E. I. Voit, A. V. Voit, A. V. Gerasimenko, and V. I. Sergienko, "Quantum chemical study of model fluorozirconate clusters," J. Struct. Chem. **41**, 41–47 (2000).
35. L. N. Ignatieva, S. a. Polishchuk, and V. M. Bouznik, "Quantum chemical and spectroscopic study of fluoride glass," Rev. Inorg. Chem. **19**, 31–44 (1999).
36. E. I. Voit, A. V. Voit, A. V. Gerasimenko, and V. I. Sergienko, "Relationship between the energy characteristics

#185229 - $15.00 USD Received 11 Feb 2013; revised 25 Mar 2013; accepted 26 Mar 2013; published 5 Apr 2013

of formation of fluorozirconates," J. Struct. Chem. **41**, 206–211 (2000).
37. Y. Kawamoto and T. Horisaka, "Short-range structures of barium, lead, and strontium meta-fluorozirconate glasses," J. Non-Cryst. Solids **56**, 39–44 (1983).
38. R. Coupé, D. Louër, J. Lucas, and A. J. Léonard, "X-ray scattering studies of glasses in the system ZrF4-BaF2," J. Am. Ceram. Soc. **66**, 523–529 (1983).
39. G. E. Walrafen, M. S. Hokmabadi, S. Guha, P. N. Krishnan, and D. C. Tran, "Low-frequency Raman investigation of lead-containing fluorozirconate glasses and melts," J. Chem. Phys. **83**, 4427–4443 (1985).
40. R. M. Almeida and J. D. Mackenzie, "A structural interpretation of the vibrational spectra of binary fluorohafnate glasses," J. Chem. Phys. **78**, 6502–6512 (1983).
41. R. M. Almeida, "Vibrational spectroscopy of glasses," J. Non-Cryst. Solids **106**, 347–358 (1988).
42. C. C. Phifer, D. J. Gosztola, J. Kieffer, and C. Austen Angell, "Effects of coordination environment on the Zr–F symmetric stretching frequency of fluorozirconate glasses, crystals, and melts," J. Chem. Phys. **94**, 3440–3450 (1991).
43. S. Aasland, M.-A. Einarsrud, T. Grande, and P. F. McMillan, "Spectroscopic investigations of fluorozirconate glasses in the ternary systems ZrF4–BaF2–AF (A = Na, Li)," J. Phys. Chem. **100**, 5457–5463 (1996).
44. R. M. Almeida and J. D. Mackenzie, "The effects of oxide impurities on the optical properties of fluoride glasses," J. Non-Cryst. Solids **56**, 63–68 (1983).
45. S. Gross, M. Ams, G. Palmer, C. T. Miese, R. J. Williams, G. D. Marshall, A. Fuerbach, D. G. Lancaster, H. Ebendorff-Heidepriem, and M. J. Withford, "Ultrafast laser inscription in soft glasses: a comparative study of athermal and thermal processing regimes for guided wave optics," Int. J. Appl. Glass Sci. **3**, 332–348 (2012).
46. J. Rousset, M. Ferrari, E. Duval, A. Boukenter, C. Mai, S. Etienne, and J. Adam, "First stages of the crystallization in fluorozirconate glasses," J. Non-Cryst. Solids **111**, 238–244 (1989).
47. M. Bernier, D. Faucher, R. Vallée, A. Saliminia, G. Androz, Y. Sheng, and S. L. Chin, "Bragg gratings photoinduced in ZBLAN fibers by femtosecond pulses at 800 nm," Opt. Lett. **32**, 454–456 (2007).
48. C. B. Schaffer, A. Brodeur, J. F. García, and E. Mazur, "Micromachining bulk glass by use of femtosecond laser pulses with nanojoule energy," Opt. Lett. **26**, 93–95 (2001).
49. D. G. Lancaster, S. Gross, H. Ebendorff-Heidepriem, K. Kuan, T. M. Monro, M. Ams, A. Fuerbach, and M. J. Withford, "Fifty percent internal slope efficiency femtosecond direct-written Tm3+:ZBLAN waveguide laser," Opt. Lett. **36**, 1587–1589 (2011).
50. R. Sramek, F. Smektala, W. Xie, M. Douay, and P. Niay, "Photoinduced surface expansion of fluorozirconate glasses," J. Non-Cryst. Solids **277**, 39–44 (2000).

1. Introduction

The unique 3-dimensional and rapid prototyping capabilities of the femtosecond (fs) laser direct-write technique [1] have drawn much attention from a diverse range of fields like telecommunication [2], quantum photonics [3], microfluidics [4], astrophotonics [5] and waveguide lasers [6]. A crucial requirement for the fs laser direct-write technique is a deeper understanding of the structural modifications induced by the fs laser pulses within the bulk dielectrics. This not only enables the optimization of the fabrication parameters and thereby the device performance [7], but also allows for materials to be tailored to offer specific properties for the direct-write process [8].

The fs laser induced structural modifications are most commonly studied using Raman microscopy and fluorescence microscopy [9–11]. So far, these modifications have been investigated for materials including silicate glasses [7, 9–15], phosphate glasses [8, 11, 16, 17] and chalcogenides [18, 19]. The type of structural modification that occurs strongly depends on the material and the exposure conditions. For instance in fused silica irradiated with kHz repetition rate fs pulses, the index change was linked to a permanent increase in the concentration of 3-member and 4-member silicon-oxygen rings [7, 9, 12]. Furthermore, a transient contribution to the index increase, which can be thermally annealed, was found and attributed to non-bridging oxygen hole centers (NBOHC) [9, 13]. In contrast, in phosphate glass, the change in refractive index was referred to a change in phosphorus-oxygen bond length and thereby densifaction/rarefaction of the glass network when using high repetition rate pulses [16], whereas after low repetition rate exposure, an increased number of Q^1 phosphorus tetrahedra (one bridging oxygen [20]) was found, that was assigned to a change in the polarizability of the glass network [17].

#185229 - $15.00 USD Received 11 Feb 2013; revised 25 Mar 2013; accepted 26 Mar 2013; published 5 Apr 2013

To date, no investigations of this type have been reported on fluoride glasses, despite their excellent optical properties [21], such as a low phonon energy which results in a high infrared transparency, and a high rare-earth solubility [22] which makes them an excellent platform for mid-infrared lasers [23]. Furthermore, these glasses feature a low nonlinearity, that limits unwanted nonlinear pulse propagation effects during the fs laser direct-write process. They also exhibit a relatively low refractive index (≈ 1.5), thereby reducing the refractive index mismatch and as such the associated spherical aberrations when focusing the writing beam into the glass [24].

In this paper we report, to the best of our knowledge, on the first study on the morphology of fs laser induced structural modifications in bulk fluorozirconate glass (ZBLAN, ZrF_4-BaF_2-LaF_3-AlF_3-NaF) using Raman microscopy.

2. Experimental methods

The ZBLAN glass with the composition 53 ZrF_4 – 20 BaF_2 – 3 LaF_3 – 4 AlF_3 – 20 NaF (mol%) was fabricated from high purity ($\geq$ 99.9%) raw materials in a controlled atmosphere glass melting facility using 50 g batch sizes [25]. For inscription of the structures a 5.1 MHz Ti:sapphire chirped pulse oscillator (FEMTOSOURCE XL 500, Femtolasers GmbH) was used. The laser operates at 800 nm and emits $<$ 50 fs pulses with a maximum pulse energy of 550 nJ. Due to the laser's high repetition rate, there is insufficient time between successive pulses for the deposited heat to diffuse out of the focal volume. As a result, an accumulation of heat occurs, which leads to melting of the glass followed by rapid quenching as the sample is moved through the tightly focused laser beam [26, 27]. The quenching time is defined by the translation speed at which the sample is moved through the focus and typically in the order of 1-10 ms [15]. The pulse train was focused by a 100$\times$ 1.25 NA oil immersion objective (Zeiss N-Achroplan) 300 μm below the surface of the sample while it was translated by computer controlled precision air bearing stages (Aerotech ABL) at a constant speed of 1000 mm/min. The laser writing beam was circularly polarized and a pulse energy of 100 nJ was used for inscription. The refractive index profile of the inscribed modifications was measured with a refracted near-field profiler (RINCK Elektronik) at 635 nm with ≈ 0.5 μm spatial resolution.

The Raman spectra were collected with a confocal Raman microscope (Renishaw Ramanscope). The instrument is equipped with motorized XYZ stages, a 785 nm diode laser for excitation and a grating spectrometer with a resolution of 1 cm^{-1}. Due to the holographic notch filter, required for blocking the Rayleigh scattered light, the minimum detectable frequency is 100 cm^{-1}. A 50$\times$ objective, providing a resolution of ≈ 2 μm, was used for spatial mapping of the inscribed structures. The ZBLAN Raman spectra were recorded from 150 to 750 cm^{-1}, accumulating ten 1 s long exposures to increase the signal to noise ratio.

2.1. Data reduction

Before performing the spectral decomposition of the Raman spectra, a detector dark frame was subtracted from the recorded data. The dark frame was obtained by acquiring a spectrum using the same exposure conditions but with the excitation laser blocked. Following this, a constant baseline was subtracted to zero the high frequency end of the acquired spectra. In the next step the spectrum was corrected for the Bose-Einstein thermal population according to [28]

$$I_R(\nu) = (1 - e^{-hc_0\nu/k_BT})I_{obs}(\nu), \tag{1}$$

where I_R is the reduced spectrum, I_{obs} the recorded spectrum, ν the Raman shift in wavenumbers, h is Planck's constant, c_0 the vacuum speed of light, k_B is the Boltzmann constant and T is the sample temperature in K. It was assumed that the sample is at room temperature (293 K)

#185229 - $15.00 USD Received 11 Feb 2013; revised 25 Mar 2013; accepted 26 Mar 2013; published 5 Apr 2013

with negligible heating from the excitation laser. Next, the spectral decomposition of the Raman spectra into their individual vibrational bands was performed by nonlinearly fitting a linear superposition of six 'pseudo-Voigt' profiles (sum of a Gaussian and Lorentzian function with identical FWHM) to the recorded data, according to

$$I_{Fit}(\nu) = \sum_{n=1}^{6} A_n \left(\mu_n \frac{w_n}{(\nu-\nu_n)^2 + w_n^2} + (1-\mu_n) e^{-\ln(2)\frac{(\nu-\nu_n)^2}{w_n^2}} \right). \quad (2)$$

The Raman shift is designated with ν, A_n is the amplitude of vibrational band n, μ is the shape factor (1...100% Lorentzian, 0...100% Gaussian), ν_n the center position and w_n the half width half maximum (HWHM) of the Raman mode. As a measure for the strength of each Raman band, the area under each peak (integrated intensity) was calculated from

$$Area = A_n \cdot \left(\mu_n \pi w_n + (1-\mu_n) w_n \sqrt{\frac{\pi}{\ln(2)}} \right). \quad (3)$$

3. Structure of fluorozirconate glass

Almeida *et al.* were the first to investigate the short range structure of fluorozirconate glass by Raman and infrared spectroscopy [29]. They looked at binary ZrF_4 – BaF_2 compositions with ZrF_4 contents ranging from 52 mol.% to 74 mol.%. They *ab inito* postulated a structural model based on zirconium fluoride polyhedra with terminal and bridging fluorine bonds, where the polyhedra are arranged in zigzag chains with single bridging fluorines (corner sharing), cross linked by Ba–F ionic bonds. By comparing their Raman spectra to fluoride crystals and using stoichiometry, they concluded for the 64 ZrF_4 – 36 BaF_2 (dizirconate) compositions (F/Zr ratio of 5.1), that the dominating structure must be ZrF_6^{2-} octahedra (coordination number (CN) 6) with 2 bridging fluorine atoms. For the 52 ZrF_4 – 48 BaF_2 (metazirconate), following comparison with the dizirconate composition, they concluded that it contains seven-coordinated Zr atoms, rather than 6, due to the higher F/Zr = 5.8 ratio (the F/Zr-ratio decreases with increasing ZrF_4 content).

A different structure for the metacirconate was proposed by Kawamoto *et al.* shortly after, suggesting that the glass is composed of ZrF_8^{4-} polyhedra with dodecahedral F coordination and partly from ZrF_7^{3-} polyhedra with monocapped trigonal prismatic F coordination [30, 31]. The polyhedra are linked to each other by sharing edges and/or corners to form a 3-dimensional network. The Ba ions serve as network modifiers, sitting in the interstices of the structure, surrounded by fluorine atoms. Their reasoning was based on Raman and differential thermal analysis of crystalline and vitreous $BaZrF_6$ and molecular dynamic simulations.

Based on computer simulations and data from X-ray scattering studies, Phifer *et al.* suggested a structural model based on Zr_2F_{13} dimers linked to rings, which form an aperiodic quasi 3-dimensional network (Fig. 1) [32]. The dimer consists of one 8-coordinated and one 7-coordinated polyhedron, sharing 2 internally binding fluorines (edge-sharing). These dimers are connected via 6 bridging fluorines (3 from each polyhedron) to each other, leaving 5 non-bridging/terminal fluorides. The terminal fluorides are in Columbic interactions with the Ba^{2+} ions, which are dispersed across the network. One shortcoming of their proposed structure is its asymmetry. This appears to contradict the observation that only a few Raman bands are present in the glass, which usually suggests high symmetry [32]. By comparison, Goncalves *et al.* proposed for 57.0 ZrF_4 – 28.1 BaF_2 – 3.3 LaF_3 – 5.0 AlF_3 – 6.6 NaF (F/Zr = 5.5) glass a structural model based on chains of alternating edge/corner sharing ZrF_7^{3-} polyhedra with Ba^{2+} as primary and Na^+ as secondary network modifiers sitting in interstitial sites.

Clearly, there is no universal model for whether zirconium fluoride glass consists of chains or a more complex 3-dimensional network of zirconium clusters. However, quantum chemical

#185229 - $15.00 USD Received 11 Feb 2013; revised 25 Mar 2013; accepted 26 Mar 2013; published 5 Apr 2013

simulations suggest that zirconium clusters with high coordination states of 7 to 8 are favorable [33–36], in agreement with the coordination numbers determined by X-ray diffraction [37,38]. These high coordination numbers require the presence of double bridging/edge-sharing links.

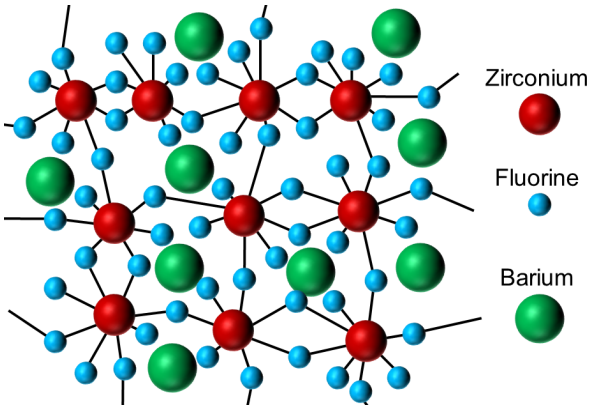

Fig. 1. Structure of the $BaZr_2F_{10}$ glass based on Zr_2F_{13} dimers (ZrF_7 and ZrF_8 polyhedra linked by a fluorine double bridges) forming a ring-like network (illustration derived from [32]).

4. Raman spectra of fluorozirconate glass

Almeida *et al.* identified five main peaks in the Raman spectrum of binary ZrF_4 – BaF_2 glass, one strong, polarized peak around $565-598$ cm^{-1}, one weaker partially polarized at $468-500$ cm^{-1}, and three weak, depolarized bands at $386-416$, $322-348$ and $183-196$ cm^{-1} [29]. The central frequency of each band depends on the composition of the glass, for instance instead of the of the ≈ 330 cm^{-1} band, Walrafen *et al.* identified a band at $\approx 230-250$ cm^{-1} in PbF_2 containing fluorzirconate [39].

The fact that there is not a unified picture of the glass structure makes the assignment of the Raman bands to different vibrations difficult and several different allocations can be found throughout the literature. The strong ≈ 580 cm^{-1} band is most widely studied and unambiguously attributed to the total symmetric stretching vibrations (ν_S) of the Zr–F_T (T…terminal fluorine bond) bonds within the polyhedra [29,30,40–43]. The next Raman mode (≈ 480 cm^{-1}) is assigned to the antisymmetric stretching vibration of the bridging fluorine bonds Zr–F_B with no movement of the heavier zirconium atoms involved [40,41]. In compliance with the occurrence of edge sharing bonds, this band was assigned by Boulard *et al.* to symmetric and antisymmetric stretching of the fluorine double bridging link [33]. Almeida *et al.* assigned the 400 cm^{-1} and 330 cm^{-1} band to motion by the non-bridging/terminal fluorine F_T, where the higher frequency band corresponds to an antisymmetric stretching and the lower frequency band to a possible 'umbrella' motion. The latter includes movement of the heavier glass forming cation, concluded by comparing spectra of similar zirconium and hafnium fluoride glasses [40]. In addition, they also noted that the lower frequency vibration (330 cm^{-1}) could be the result of skeletal bending of the bridging fluorine atoms F_B with displacement of the zirconium due to its slightly different frequency in fluorohafnate glass. However, the fact that the 330 cm^{-1} band does not lose intensity upon melting makes it likely due to motion of terminal fluorines F_T rather than bridging fluorine F_B [39]. In contrast, the 400 cm^{-1} band intensity decreases when heated and therefore it should be assigned to bridging rather than terminal fluorine atoms [39]. The lowest frequency Raman band (≈ 190 cm^{-1}) was assigned to a skeletal bending vibration

#185229 - $15.00 USD Received 11 Feb 2013; revised 25 Mar 2013; accepted 26 Mar 2013; published 5 Apr 2013

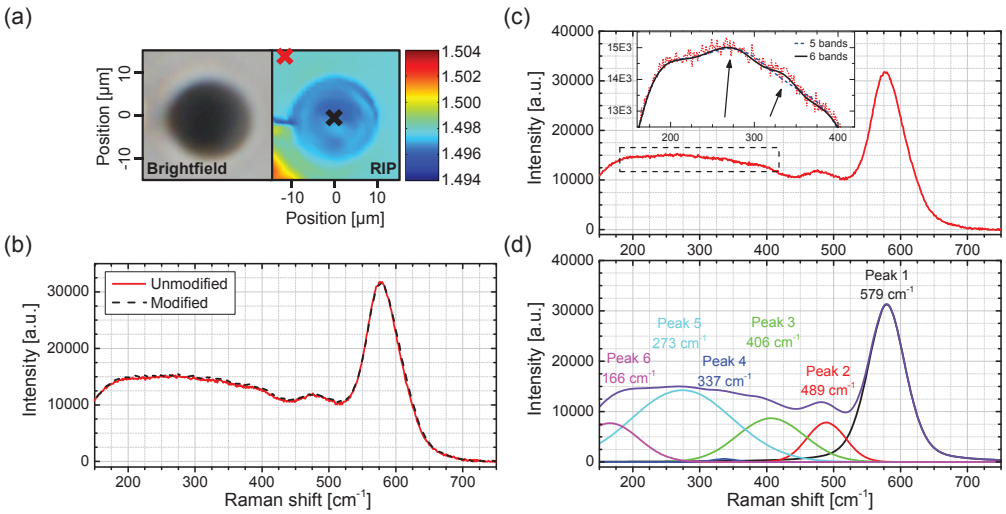

Fig. 2. (a) Optical microscope image and corresponding refractive index profiles (RIP) of the analyzed modification with an average refractive index change of $\Delta n = (-1.0 \pm 0.2) \times 10^{-3}$ in its center. The black and red cross in the RIP indicate the approximate location of the collected spectra shown below. (b) Raman spectra of unmodified and modified ZBLAN plotted on top of each other, illustrating the only very subtle changes in Raman response between modified and unmodified ZBLAN. (c) Raman spectra of unmodified ZBLAN. The inset highlights an additional weak band at ≈ 335 cm^{-1} arising from impurities. For comparison, the deconvolved spectrum is shown for a curve fit using 5 and 6 bands. (d) Spectral decomposition into 6 bands of the Raman spectrum illustrated in (c).

composed of a symmetric stretching by bridging fluorines with zirconium motion [40, 41] and in compliance with this assignment to bridging bonds, Walrafen *et al.* demonstrated a decrease in intensity upon heating [39].

5. Experimental results

A brightfield microscope image of the investigated laser modification inscribed with 100 nJ pulse energy at a translation speed of 1000 mm/min is depicted in Fig. 2a. Next to the microscope image in Fig. 2a is the corresponding refractive index profile (RIP), showing an average refractive index change of $\Delta n = (-1.0 \pm 0.2) \times 10^{-3}$ in its center. Two crosses in the RIP indicate the location at which the Raman spectra shown in Fig. 2b of the unmodified (solid red line) and modified glass (dashed black line) were collected. Figure 2c shows the recorded spectra after correction for the detector dark current, the Bose-Einstein thermal population and subtraction of a constant background to set the long frequency tail to zero. The decomposition of the Raman spectrum into the Raman bands, as identified by Almeida *et al.*, is shown in Fig. 2d. Additionally, a weak band at ≈ 330 cm^{-1}, next to the 270 cm^{-1} feature, was found as indicated by the arrows in the inset of Fig. 2c. This extra band could arise from oxygen impurities as seen in spectra of 56.3 ZrF_4 – 34.7 BaF_2 – 7.0 ThF_4 glass, which was deliberately doped with ZrO_2 [44]. This band is also present in spectra recorded from locations several tens of microns deep within the bulk glass, which excludes oxidation/corrosion of the surface as cause. The inset in Fig. 2c shows the deconvolved spectrum when fitting 5 bands and 6 bands, respectively. In order for the deconvolved spectra to closest represent the experimental data, this additional weak band at ≈ 335 cm^{-1} was included in the curve fitting process. Without this band, the ≈ 270 cm^{-1} Raman peak converged to a higher frequency, slightly off the peak po-

#185229 - $15.00 USD Received 11 Feb 2013; revised 25 Mar 2013; accepted 26 Mar 2013; published 5 Apr 2013

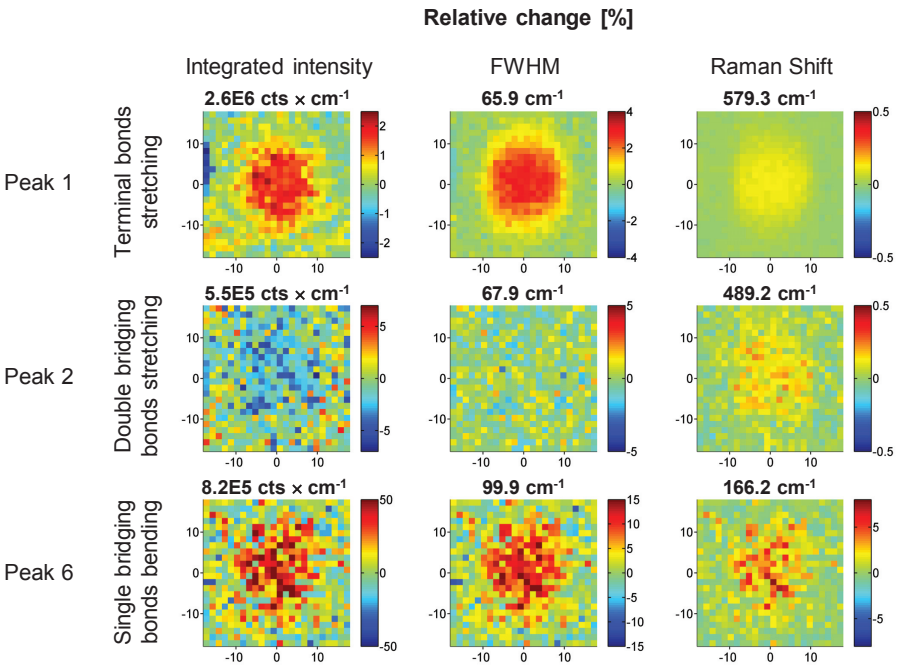

Fig. 3. Spatially resolved Raman data of a laser induced modification from Fig. 2a. Each row corresponds to one Raman peak, with column one being its integrated intensity (area underneath the curve), column two shows the change in FWHM and column three illustrates the shift in center frequency. The data is the relative percentage change normalized against the bulk glass.

sition in the recorded spectra, as well as a larger FWHM was observed compared to the case with 6 bands. Since the amount of impurities is not expected to change in the laser modified region, the ≈ 335 cm^{-1} band was kept constant during the curve fitting process using the curve parameters of pristine glass.

Since band 3 and 5 are only weakly pronounced and do not have any distinctive features in the spectrum, a careful choice of the initial values for the fitting parameters was necessary to obtain reproducible outcomes. However, the obtained fitting parameters, in particular amplitude and width, for those bands were associated with large confidence bounds resulting in a large variation from fit to fit and as such a low signal-to-noise ratio.

The absence of any sharp peaks in the Raman spectrum of the modified glass indicates that the vitreous state is preserved after being heated above the melting point by the laser and quenched to room temperature on a millisecond timescale. Furthermore, the laser modified volume is transparent with no scattering being observed when investigating the structures under the optical microscope with crossed polarizers [45]. For Raman bands similar to the polycrystalline phase to evolve, the glass has to be kept at a temperature close to the glass transition temperature for several hundred hours which then results in the formation of crystallites of 75 Å average size [46].

To spatially resolve the entire inscribed structure depicted in Fig. 2a, a raster scan was performed, recording Raman spectra across a 36×36 μm window with 1.5 μm step size in x and y. Those Raman bands of the glass network, that spatially reflect the shape of the refractive index modification are shown in Fig. 3. As mentioned above, the maps for Raman band 3 and 5

#185229 - $15.00 USD Received 11 Feb 2013; revised 25 Mar 2013; accepted 26 Mar 2013; published 5 Apr 2013

were very noisy due to the large confidence bounds of the fit. Therefore, subtle changes in band 3 and 5 are potentially obscured by noise arising from the curve fitting.

The maps in Fig. 3 show the relative change in percentage compared to the bulk glass background, which was taken as the average over a 5 by 5 pixel square from each corner. The bulk glass reference value for each parameter is noted at the top of each map. The first column in Fig. 3 shows the relative change in integrated intensity (area underneath the curve). The relative percentage change in FWHM and Raman shift for each band are shown in the second and third column, respectively.

The intensity of the 580 cm^{-1} Raman band (peak 1) increases in the laser modified regions by $(+1.5 \pm 0.4)$%, indicating an increase in terminal bonds. The increase in terminal bonds must be accompanied by a decrease in bridging bonds. This is reflected by a relative drop in intensity by (-1.8 ± 1.6)% (column 1/row 2) of the 480 cm^{-1} band, which has been assigned to stretching of the double bridging fluorine bonds. In turn, an increase in the intensity of the skeletal bending mode by $(+28 \pm 20)$% (peak 6), which has been attributed to single bridging fluorine, is observed (column 1/row 3). As a consequence of the decrease in strength of the double bridging fluorine and increase in the single bridging fluorine Raman bands, a fraction of the double bridging bonds must have been broken up into single bridging ones. Under conservation of the total number of fluorine atoms situated around zirconium, the coordination number of one of the two zirconium polyhedra, which previously were linked by a double bridging bond, has to decrease while the coordination number of the second polyhedra stays the same. A decrease in coordination number results in an increase of the 580 cm^{-1} band frequency [42], and indeed an increase in Raman shift is observed, as illustrated by the map in column 3, row 1. The 580 cm^{-1} band (peak 1) is sufficiently broad to account for the symmetric stretching vibrations of several different ZrF_n^{4-n} species and as such splitting is not expected [39]. However, the change in coordination number of some zirconium polyhedra results in a changed spread of zirconium coordination numbers. Hence, a change in the width of peak 1 is expected and indeed, the FWHM of peak 1 increases as shown in column 2/row 1. It should be noted that a decrease in the number of bridging bonds leads to a decrease in frequency of peak 1. However, the effect of the change in the coordination number is stronger than the change due to bridging [42]. The increased frequency of peak 6 suggests either a decreased bond angle or a reduced single bridging bond length in the laser modified volume [40]. However, because there is no unified picture of the glass network makes a definitive assignment to either one of the effects difficult.

Based on these observations we can postulate the following picture: The tightly focused high repetition rate fs pulse train results in local melting of the glass and thus breaking of the bridging bonds. This is followed by rapid quenching on a millisecond timescale as the sample is moved through the focus of the laser beam. As the glass resolidifies, a larger fraction of single bridging fluorine bonds relative to double bridging bonds are formed than there were present in the pristine glass, which solidified significantly slower on a minute timescale. The distance between neighboring zirconium cations for single bridging/corner-sharing bonds is larger than in the case of double bridging/edge-sharing bond (4.15 Å for single bridging compared to 3.56 Å for double bridging in the case of α-ZrF_4 consisting of triangular dodecahedron ZrF_8 polyhedra [31]). Therefore, the glass network is less efficiently packed and exhibits a decreased density, resulting in a decreased refractive index via the Lorentz-Lorenz equation.

ZBLAN not only responds with a negative index change to high repetition rate 800 nm fs radiation but also when exposing it to kHz repetition rate pulses [45, 47]. At first glance, one interpretation is that the index change for high and low pulse repetition rate exposure have the same underlying mechanisms. However, the thermal conditions between the two regimes are significantly different with the glass being quenched on a microsecond timescale (≈ 1 μs is

#185229 - $15.00 USD Received 11 Feb 2013; revised 25 Mar 2013; accepted 26 Mar 2013; published 5 Apr 2013

the typical thermal diffusion time of glass [48]) in the kHz regime as opposed to milliseconds in the MHz regime. For instance while in borosilicate glass, both regimes result in a positive index change, the underlying structural modifications of the glass network are different [15]. The index change in borosilicate glass for low repetition rates was attributed to the formation of non-bridging oxygen atoms, whereas density changes were found as dominating cause for the index change in the high repetition rate regime. In the case of ZBLAN different bond breakage and/or structural rearrangement may occur in the kHz regime and/or the even faster cooling rate freezes in a structure that could not be frozen in with the slower cooling rate in the MHz repetition rate regime. Future work will investigate the structural changes in the kHz region.

The rarefaction of the glass network is consistent with the presence of stress induced by the laser modified regions and the occurrence of stress fractures [49]. An expansion of the glass network was also observed by Sramek *et al.*, when irradiating the surfaces of several different fluorozirconate glasses with pulsed 193 nm radiation [50].

The structural modification of the glass network was related to changes in the bridging bonds linking zirconium fluoride polyhedra. This provides a potential avenue for tailoring the photo response of fluorozirconate glass by adjusting the fluorine to zirconium ratio of the glass composition. Substituting ZrF_4 by BaF_2 and vice versa increases/decreases the F/Zr ratio. Aasland *et al.* showed, that the F/Zr ratio influences the bridging between zirconium fluoride polyhedra and their coordination number [43]. This was reflected in a relative intensity change between the 580 cm^{-1} and 480 cm^{-1} Raman bands and a shift in frequency of both bands.

6. Conclusion

We used Raman microscopy to reveal the underlying structural changes of the ZBLAN glass network after exposure to high repetition rate 800 nm fs pulses. The laser results in local melting followed by rapid quenching of the glass. As the glass resolidifies, a larger fraction of single bridging fluorine bonds relative to double bridging bonds are formed compared with the pristine (slowly cooled) glass. The distance between neighboring zirconium cations is larger in the case of single bridging bonds which results in a rarefaction of the glass network. This can be related to the observed decrease in refractive index via the Lorentz-Lorenz equation. These findings are an important step towards tailoring the photo response for the fs direct-write process of fluorozirconate glass via engineering the glass composition.

Acknowledgments

We would like to acknowledge Krystyna Drozdowicz-Tomsia for her assistance with operating the Raman microscope. This research was supported by the Australian Research Council Centre of Excellence for Ultrahigh bandwidth Devices for Optical Systems (project number CE110001018) and was performed in part at the OptoFab node of the Australian National Fabrication Facility utilizing Commonwealth, NSW, and SA State Government funding. S. Gross acknowledges support by the iMQRES scholarship. T. Monro acknowledges the support of an ARC Federation Fellowship.

#185229 - $15.00 USD Received 11 Feb 2013; revised 25 Mar 2013; accepted 26 Mar 2013; published 5 Apr 2013